IOPscience iopscience.iop.org

Home Search Collections Journals About Contact us My IOPscience

Inclusion of thin target and source regions in alimentary and respiratory tract systems of mesh-type ICRP adult reference phantoms

This content has been downloaded from IOPscience. Please scroll down to see the full text.

2017 Phys. Med. Biol. 62 2132

(http://iopscience.iop.org/0031-9155/62/6/2132)

View the table of contents for this issue, or go to the journal homepage for more

Download details:

IP Address: 146.107.3.4
This content was downloaded on 28/02/2017 at 07:56

Please note that terms and conditions apply.

You may also be interested in:

Development of skeletal system for mesh-type ICRP reference adult phantoms
Yeon Soo Yeom, Zhao Jun Wang, Thang Tat Nguyen et al.

Conversion of ICRP male reference phantom to polygon-surface phantom
Yeon Soo Yeom, Min Cheol Han, Chan Hyeong Kim et al.

New small-intestine modeling method for surface-based computational human phantoms
Yeon Soo Yeom, Han Sung Kim, Thang Tat Nguyen et al.

Incorporation of detailed eye model into polygon-mesh versions of ICRP-110 reference phantoms
Thang Tat Nguyen, Yeon Soo Yeom, Han Sung Kim et al.

Electron specific absorbed fractions for the adult male and female ICRP/ICRU reference computational phantoms
Maria Zankl, Helmut Schlattl, Nina Petoussi-Henss et al.

Hybrid newborn computational phantoms
Choonsik Lee, Daniel Lodwick, Deanna Hasenauer et al.

Comparison of internal dosimetry factors for three classes of adult computational phantoms
Stephanie Lamart, Andre Bouville, Steven L Simon et al.

Application of the ICRP/ICRU reference phantoms to internal dosimetry
L Hadid, A Desbrée, H Schlattl et al.

Organ dose conversion coefficients for reference adult male and female
H Schlattl, M Zankl and N Petoussi-Henss

IOP Publishing | Institute of Physics and Engineering in Medicine Physics in Medicine & Biology

Phys. Med. Biol. **62** (2017) 2132–2152 doi:10.1088/1361-6560/aa5b72

Inclusion of thin target and source regions in alimentary and respiratory tract systems of mesh-type ICRP adult reference phantoms

Han Sung Kim[1], Yeon Soo Yeom[1], Thang Tat Nguyen[1], Chansoo Choi[1], Min Cheol Han[1], Jai Ki Lee[1], Chan Hyeong Kim[1], Maria Zankl[2], Nina Petoussi-Henss[2], Wesley E Bolch[3], Choonsik Lee[4], Rui Qiu[5], Keith Eckerman[6] and Beom Sun Chung[7]

[1] Department of Nuclear Engineering, Hanyang University, Seoul, Korea
[2] Research Unit Medical Radiation Physics and Diagnostics, Helmholtz Zentrum München Deutsches Forschungszentrum für Gesundheit und Umwelt (GmbH), Neuherberg, Germany
[3] J Crayton Pruitt Family Department of Biomedical Engineering, University of Florida, Gainesville, FL, United States of America
[4] Division of Cancer Epidemiology & Genetics, National Cancer Institute, National Institutes of Health, Bethesda, MD, United States of America
[5] Department of Engineering Physics, Tsinghua University, Beijing, People's Republic of China
[6] Oak Ridge National Laboratory, Oak Ridge, TN, United States of America
[7] Department of Anatomy, Ajou University School of Medicine, Suwon, Korea

E-mail: chkim@hanyang.ac.kr

Received 29 November 2016, revised 18 January 2017
Accepted for publication 23 January 2017
Published 17 February 2017

Abstract

It is not feasible to define very small or complex organs and tissues in the current voxel-type adult reference computational phantoms of the International Commission on Radiological Protection (ICRP), which limit dose coefficients for weakly penetrating radiations. To address the problem, the ICRP is converting the voxel-type reference phantoms into mesh-type phantoms. In the present study, as a part of the conversion project, the micrometer-thick target and source regions in the alimentary and respiratory tract systems as described in ICRP *Publications 100* and *66* were included in the mesh-type ICRP reference adult male and female phantoms. In addition, realistic lung airway models were simulated to represent the bronchial (BB) and bronchiolar (bb) regions. The electron specific absorbed fraction (SAF) values for the

 © 2017 Institute of Physics and Engineering in Medicine Printed in the UK

alimentary and respiratory tract systems were then calculated and compared with the values calculated with the stylized models of ICRP *Publications 100* and *66*. The comparisons show generally good agreement for the oral cavity, oesophagus, and BB, whereas for the stomach, small intestine, large intestine, extrathoracic region, and bb, there are some differences (e.g. up to ~9 times in the large intestine). The difference is mainly due to anatomical difference in these organs between the realistic mesh-type phantoms and the simplified stylized models. The new alimentary and respiratory tract models in the mesh-type ICRP reference phantoms preserve the topology and dimensions of the voxel-type ICRP phantoms and provide more reliable SAF values than the simplified models adopted in previous ICRP *Publications*.

Keywords: specific absorbed fraction, alimentary tract system, respiratory tract system, ICRP reference phantom, mesh phantom, Monte Carlo

(Some figures may appear in colour only in the online journal)

1. Introduction

In the 2007 Recommendations, the International Commission on Radiological Protection (ICRP) adopted adult male and female reference computational phantoms for calculation of reference dose coefficients (ICRP 2007). The ICRP adult reference phantoms are described in ICRP *Publication 110* (ICRP 2009). These phantoms are constructed from the whole-body computed tomography (CT) images of a male and female patient with external dimensions close to the reference size of ICRP *Publication 89* (ICRP 2002). They consist of a large number of volume elements (i.e. voxels) of dimension of $2.137 \times 2.137 \times 8\,\mathrm{mm}^3$ for the male and $1.775 \times 1.775 \times 4.84\,\mathrm{mm}^3$ for the female. Although representing the human anatomy more realistically than the mathematical (or stylized) phantoms, the ICRP-110 reference phantoms, due to their limited voxel resolutions, have limitations in representing small or complex organs and thin tissues such as the lens of the eye, skeletal tissues, and a basal layer of the skin. These limitations eventually could induce problems in dose coefficient calculation particularly for weakly penetrating radiation.

For example, the voxel-type ICRP-110 phantoms cannot include the tens-of-micrometer-thick radiosensitive target and source regions of the alimentary and respiratory tract systems as prescribed in ICRP *Publication 100* (ICRP 2006) and *Publication 66* (ICRP 1994), respectively. For exposures of the ICRP-110 phantoms, therefore, doses for these organs are approximated by averaging the absorbed dose over the entire volume of an organ, instead of over the thin target region. Although this approximation provides reliable doses for most highly-penetrating radiation (e.g. photons and neutrons), it is no longer reliable for weakly-penetrating radiation (e.g. beta and alpha particles) which shows very high dose gradient in medium. Acknowledging this limitation, the ICRP additionally used a total of 11 stylized models (ICRP 1994, 2006, 2015, 2016) to calculate charged-particle specific absorbed fractions (SAFs) for the alimentary and respiratory tract organs. In the stylized models, the alimentary and respiratory tract organs were simplified to mathematical shapes such as a sphere or a cylinder, including the thin target and source regions. Although the separate use of the stylized models, in addition to the ICRP-110 phantoms, at least enabled the calculation of SAFs for the alimentary and respiratory tract systems considering the thin target and source regions, this approach leads to other issues: inherent inconsistencies in dose coefficients due

to the use of different models for different radiation types and more complicated calculation process. Moreover, the stylized models, which are technically impossible to be installed in the voxel-type ICRP-110 reference phantoms, cannot be used for the calculation of crossfire dose, i.e. the dose contribution to the thin target of the respiratory or alimentary tract organs resulting from decay of radionuclides located in other organs and, vice versa, the dose contribution from decay of radionuclides located in the thin source regions of the respiratory and alimentary tract systems to other target regions.

In order to address the aforementioned limitations and others of the voxel-type ICRP-110 reference phantoms in dose-coefficient calculations, the ICRP recently formed a Task Group (i.e. Task Group 103) to convert the voxel-type ICRP-110 reference phantoms into a high-quality mesh format. The objectives of the conversion project are to convert the voxel-type ICRP-110 reference phantoms into a high-quality mesh format faithfully preserving the original anatomical structures of the ICRP-110 phantoms and also to add all fine structures including the thin target and source regions of the alimentary and respiratory tract systems of the converted phantoms. The success of the project will provide a single set of mesh-type ICRP reference phantoms that can be used to calculate all the necessary dose coefficients for both external and internal exposures.

As a part of the conversion project, in the present study, the thin target and source regions of the alimentary and respiratory tract organs were modeled in the mesh-type ICRP reference phantoms, following the morphometric data given in ICRP *Publication 89* (ICRP 2002), *Publication 100* (ICRP 2006), and *Publication 66* (ICRP 1994). Realistic lung airway models were also generated to represent the bronchial (BB) and bronchiolar (bb) regions in the phantoms. Then, the mesh-type phantoms with the thin target and source regions were used to calculate electron SAF values for the alimentary and respiratory tract organs, and the calculated values were compared with the values calculated with the stylized models described in ICRP *Publication 100* (ICRP 2006) and *Publication 66* (ICRP 1994).

2. Material and methods

2.1. Mesh-type ICRP adult reference phantoms

The present study defined the target and source regions in the alimentary and respiratory tract organs of the mesh-type ICRP reference adult phantoms under development (figure 1). Most of the organs of the mesh phantoms were constructed by directly converting the ICRP-110 voxel models into a high-quality polygon-mesh (PM) format via 3D surface rendering and several refinement processes by using several 3D programs. The complex organs, which cannot be directly converted to high-quality PM models, were constructed by modeling methods (Nguyen *et al* 2015, Kim *et al* 2016, Yeom *et al* 2016a). For example, a detailed eye model of Behrens *et al* (2009) adopted in ICRP *Publication 116* (ICRP 2010) was produced in a PM model and incorporated into the mesh phantoms (Nguyen *et al* 2015). The lymph nodes were generated in the mesh phantoms by using a modeling approach based on the lymph node data established to generate lymph nodes in the UF/NCI family phantoms (Lee *et al* 2007, Kim *et al* 2016). The organs that have not been yet constructed were temporally filled with residual soft tissue (RST) (Lee *et al* 2007, Kim *et al* 2011, Yeom *et al* 2013). All of the alimentary tract organs in the mesh phantoms were directly converted from the ICRP-110 reference phantoms with the only exception of the small intestine. The small intestine was constructed by using a dedicated modeling method developed by Yeom *et al* (2016b) and installed in the mesh phantoms. For the respiratory tract organs, the exterior boundaries of the lungs and the

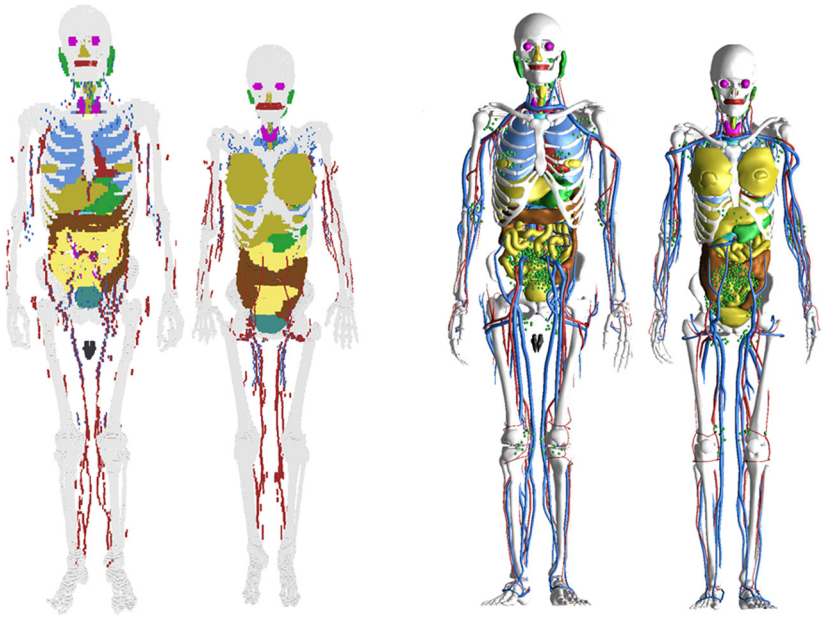

Figure 1. Voxel-type ICRP-110 reference computational phantoms (left) and mesh-type ICRP reference computational phantoms under development (right).

extrathoracic (ET) region in the mesh phantoms were also directly converted from the ICRP-110 phantoms.

2.2. Definition of target and source regions in alimentary tract organs of mesh phantoms

Based on the morphometric data provided in ICRP *Publication 100* (ICRP 2006), the target and source regions of the alimentary tract organs were defined in the mesh-type ICRP reference phantoms. For all organs except for the oral cavity (i.e. oesophagus, stomach, small intestine, and large intestine), the target and source regions were defined mainly using the *offset* function of *Rapidform* software (INUS Technology Inc., Korea). This function is used to shrink or enlarge a mesh model in the normal vector directions of the facets in the mesh, which allows for the creation of surfaces to define the tens-of-micrometer-thick target and source regions at a specific depth from the surface of the lumens.

For the oral cavity, which is geometrically more complicated than the other alimentary tract organs, the target and source regions were defined using several functions of *Rapidform* software (i.e. *offset*, *divide*, and *thicken*). Two source regions were defined: source in food (or liquid) and source retained on the surface of the teeth. The food as potential source with volume of 20 cm^3 should be placed on the tongue, but in the ICRP reference phantoms, there is no space to define the food; therefore, the tongue was divided into upper and lower part using the *divide* function, and then, only for the purpose of SAF calculation, it was assumed that the upper part is the food region. The teeth-retained radionuclides were defined by adding a 10 μm layer on the surface of the teeth using the *thicken* function. The target layer in the oral mucosa was defined in three parts: tongue, roof of mouth, and lip and cheek. The target layer in the tongue was modeled at a depth of 190–200 μm from the bottom surface of the food by using the *offset* function. The target layer in the roof was modeled by defining a 10 μm layer at a depth of 190 μm from the top surface of the food using the *offset* and *thicken* functions.

Similarly, the target layer in the lip and cheek was modeled by defining a 10 μm layer at a depth of 190 μm from the surface of the outer part of the retained source regions.

The reference value for the oesophageal content is not given in ICRP *Publication 89* (ICRP 2002); thus, the ICRP-110 reference phantoms do not include the oesophageal lumen, and calculation of SAFs for the oesophagus as source region is not possible. In the present study, therefore, we added the lumen in the oesophagus, assigning the same volume as the ICRP-100 stylized models (male: 22.0 cm^3 and female: 20.4 cm^3). For this change, both the length and diameter of the oesophagus had to be increased by ~0.3 cm, its total volume being increased by ~1.5 times, for both the male and female phantoms, which we believe would not significantly affect dose calculation for highly penetrating radiations. This process resulted in the reduction of RST, keeping the total body weight unchanged.

Figure 2 shows some examples of the target regions defined in the alimentary tract organs of the male phantom. Tables 1 and 2 provide detailed information on the source and target regions of the alimentary tract organs modeled in the present study, along with the data of the ICRP-100 stylized models and ICRP-89 reference data.

2.3. Definition of target and source regions in respiratory tract organs of mesh phantoms

Based on the morphometric data provided by ICRP *Publication 66* (ICRP 1994), the target and source regions were also defined in the respiratory tract organs, i.e. extrathoracic (ET_1 and ET_2), bronchial (BB), bronchiolar (bb), and alveolar-interstitial (AI) region of the mesh-type ICRP reference phantoms. For the ET_1 and ET_2, present in the ICRP-110 reference phantoms, the target and source regions were defined using the *offset* function following the same method used for the alimentary tract organs.

The AI was not defined separately but simply considered as the lungs except for the BB and bb regions in the mesh phantoms, taking into account the statement of the ICRP *Publication 66* (ICRP 1994): '*(313) In the AI region, the interalveolar septa and the walls of blood and lymphatic capillaries are sufficiently thin to ensure that sensitive target cells are distributed homogenously throughout the tissue mass. Therefore, it can be assumed that the average dose received by the target cells is the same as that received by the whole tissue mass'*.

The main BBs (=generation 1) in the ICRP-110 phantoms were distinguishable and thus were directly converted to the PM format, after which the target and source regions were defined using the *offset* function. For construction of the rest generations (i.e. airway generations 2–8) of the BBs and the all generations of bbs (i.e. airway generation 9–15), a dedicated computer program was developed based on a branching generation algorithm (Tawhai *et al* 2000). Figure 3 shows a flowchart of the developed program. The program first imports the phantom data: the lung PM model, the starting point, and the diameters and lengths of each branch generation. Then, a large number of points ($=10^6$) are randomly generated in the lung PM model and a centroid is calculated by averaging the coordinates of the points. A branch-center line is then generated from the starting point toward the centroid and the length is randomly determined but larger than the diameter and less than the length of the segment defined by the starting point and the centroid. For the next airway generation, the space of the lung PM model is divided by using the imaginary plane containing the centroid and the mother branch-center line. Again, a centroid of the divided space is calculated by averaging the coordinates of the points within the space and a branch-center line is generated from the ending point of the mother branch-center line toward the centroid. This procedure is repeated until the total length for each generation reaches the reference value (ICRP 1994). Note that the branch candidates, overlapped with the previously generated branches or the boundary of the lung, are rejected.

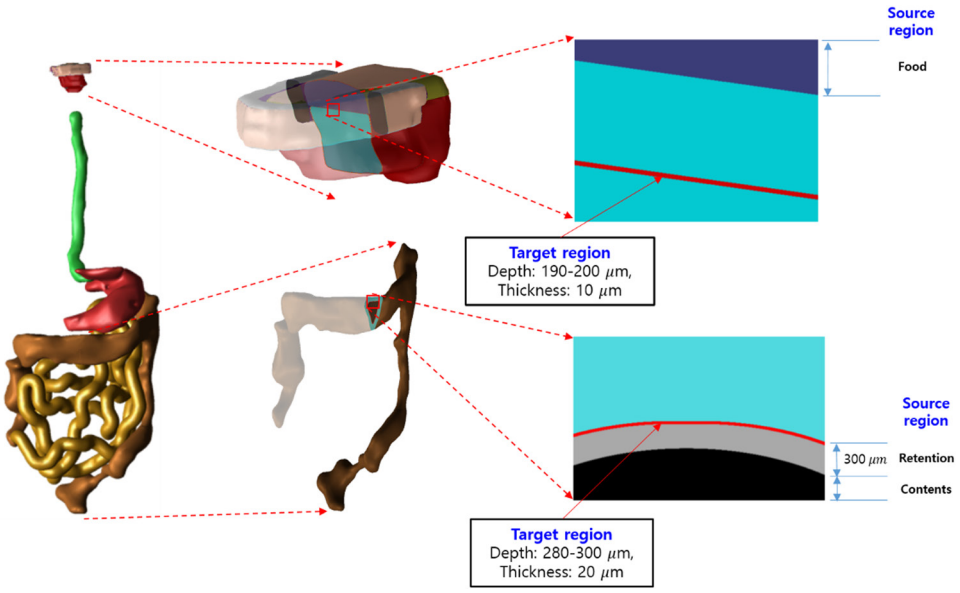

Figure 2. Target and source regions defined in alimentary tract of male phantom: oral cavity (upper) and large intestine (lower).

Table 1. Masses of source regions of alimentary tract organs of mesh-type ICRP reference phantoms and ICRP-100 stylized models; for comparison, the ICRP-89 reference data are also shown.

		Mass (g)					
		Male			Female		
Alimentary tract organ	Source region	ICRP-100	Mesh	ICRP-89	ICRP 100	Mesh	ICRP-89
Oral cavity	Food	20.0	20.8	—	20.0	20.8	—
	Retention on teeth	0.043	0.043	—	0.043	0.036	—
Oesophagus	Contents	22.0	22.9	—	20.4	21.2	—
	Lumenal surface	—	—	—	—	—	—
Stomach	Contents	175.0	250.0	250	175.0	230.0	230
	mucosa	4.6	9.8	—	4.6	7.9	—
Small intestine	Contents	879.6	350.0	350	816.8	280.0	280
	Villi	85.8	53.3	—	79.6	44.4	—
	Mucosa	35.5	22.6	—	33.0	18.8	—
Right colon	Contents	961.3	150.0	150	848.2	160.0	160
	Mucosa	19.3	7.6	—	17.0	8.8	—
Left colon	Contents	746.1	75.0	75	687.2	80.0	80
	Mucosa	18.0	6.0	—	16.6	5.6	—
Rectosigmoid	Contents	268.6	75.0	75	247.4	80.0	80
	Mucosa	10.9	4.8	—	10.0	4.5	—

Table 2. Target regions of alimentary tract organs of mesh-type ICRP reference phantoms and ICRP-100 stylized models.

		Mass (g)			
		Male		Female	
Alimentary tract organ	Target region depth (μm)	ICRP-100	Mesh	ICRP-100	Mesh
Oral cavity	190–200	0.23	0.131	0.23	0.099
Oesophagus	190–200	0.091	0.102	0.085	0.097
Stomach	60–100	0.62	1.297	0.62	1.048
Small intestine	130–150	3.568	2.271	3.313	1.895
Right colon	280–300	1.294	0.513	1.142	0.590
Left colon		1.208	0.409	1.112	0.381
Rectosigmoid		0.730	0.324	0.672	0.307

This rejection is inevitable to avoid the overlapping problems but rarely occurs in the early generation branches, generating a sufficiently complex tree structure.

Next, the generated branch-center lines were used to construct the airway models in a constructive solid geometry (CSG) format, which are based on an inverted Y-shape model as shown in figure 4. The inverted Y-shape model is represented as a union geometry of spheres and truncated cones. The spheres are located at the end of the branch-center lines and their diameters correspond to the branch diameters for each generation. The truncated cones are located between the mother and daughter spheres. The upper and lower diameters of the truncated cones are automatically determined to be tangent to both spheres. The use of the inverted Y-shape model not only makes it possible to connect the surfaces of all of the branches but also to define the micrometer-thick target and source layers, simply changing the sphere diameters (i.e. branch diameters) (Lazaro 2011).

Note that the airway generation algorithm developed in the present study relies on a random process, and different runs of this algorithm will produce different airway tree models, resulting in different SAF values. The differences are, however, expected to be marginal considering that due to the nature of the algorithm, the airway branches tend to be homogeneously distributed within the lungs.

Figure 5 shows the airway model produced in the lungs of the male PM phantom along with the original voxel model of the ICRP-110 male phantom. It can be seen that the airway models of the PM phantoms significantly improve the anatomical realism of the complex tree structure as compared to those of the voxel phantoms, at the same time representing the thin target and source layers correctly. Table 3 shows the total length of branches for each generation for the constructed airway models along with the reference values. It can be seen that both values are in good agreement; that is, the discrepancies are less than 10% for all generations.

Table 4 compares the target masses of respiratory tract organs of the PM phantoms with those of ICRP-66 stylized models. For the ET_1 and ET_2, the target-mass differences were almost 40% and 80%, respectively. The significant differences are again due to the difference in the ET shapes between the PM phantoms and the stylized models, more specifically the inner surface areas which determine the target masses. For the BB and bb, on the other hand, the target-mass differences were much less significant, i.e. within the range from 11% to 23%. It can be also seen that the target masses of the PM phantoms tend to be smaller than those of the stylized models. This tendency of the PM phantoms would be more reasonable,

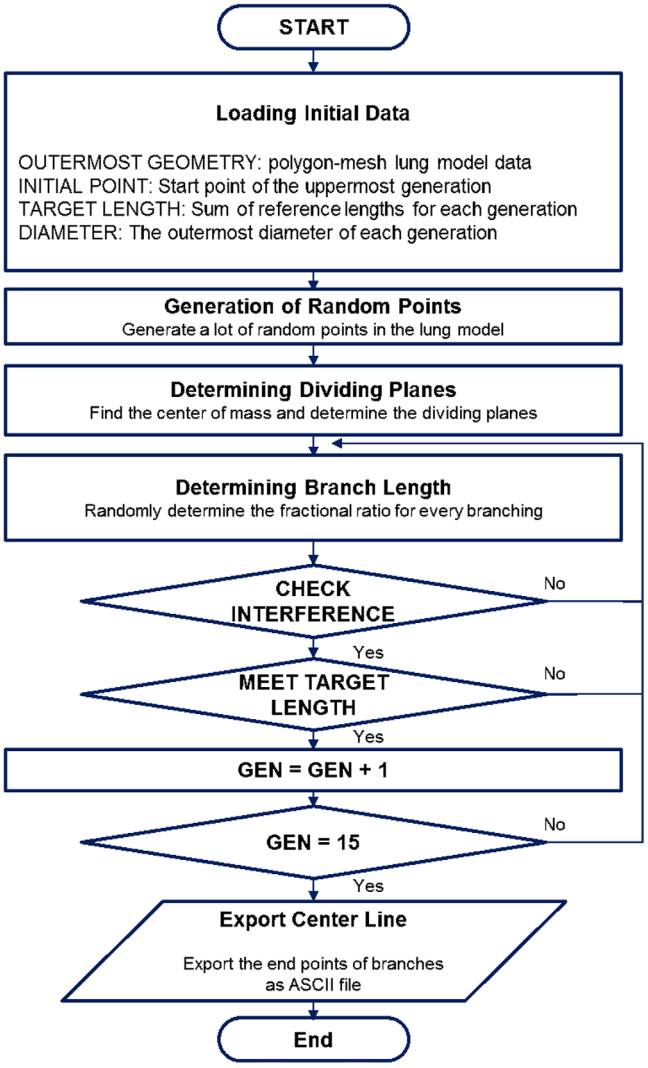

Figure 3. Flowchart of the developed program for generation of center lines of lung airways.

considering that the overlaps of the mother and daughter branches are considered in the developed PM phantoms but not in the ICRP-66 cylindrical models.

2.4. Monte Carlo simulations

Monte Carlo radiation transport simulations were performed to calculate the electron SAF values for the alimentary and respiratory tract systems of the mesh-type ICRP reference phantoms including the thin target and source regions in the alimentary and respiratory tract systems. Then, the calculated SAF values were compared with those calculated by using the ICRP-100 and ICRP-66 stylized models in order to investigate dose differences caused by the different topology and dimension of the alimentary and respiratory tract systems between the mesh phantoms and the stylized models. For the simulation, the Geant4 code (ver. 10.01)

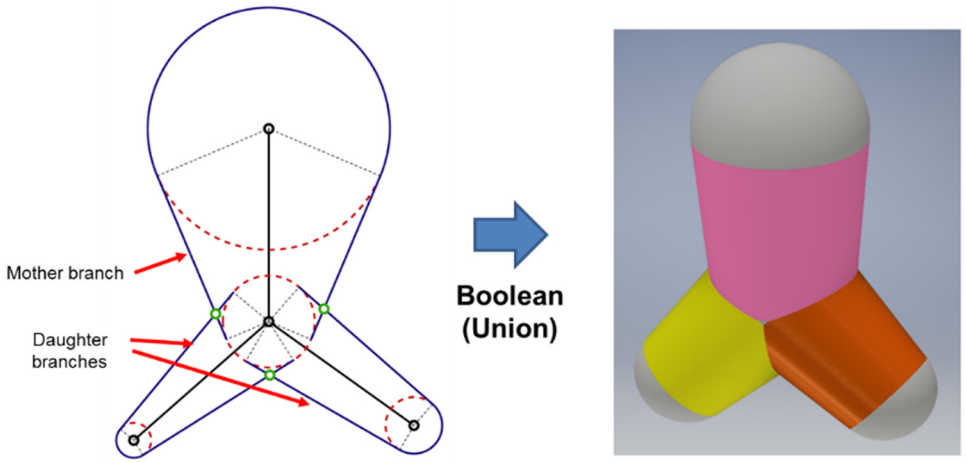

Figure 4. Inverted Y-shape model in the constructive solid geometry (CSG) format.

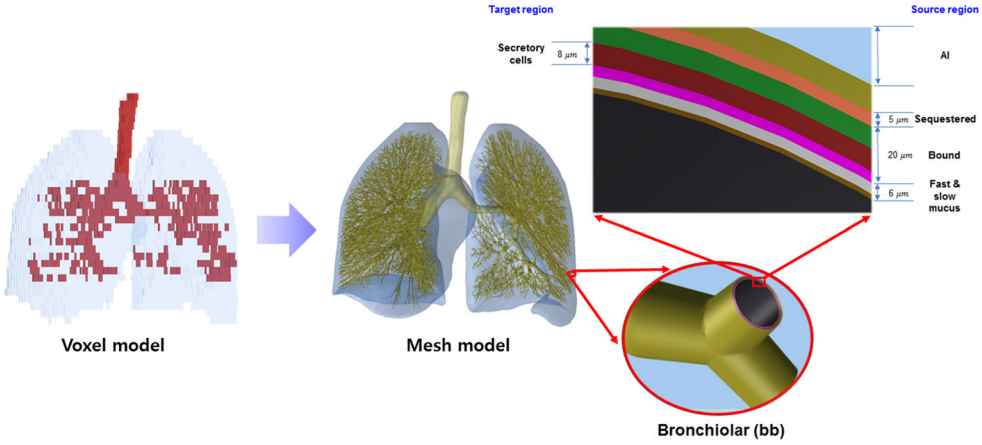

Figure 5. Lung voxel model (left) and lung PM model (right) for the male phantom.

(Agostinelli *et al* 2003) was used. To improve the computation speed, the mesh phantoms of the PM format were converted to the tetrahedral-mesh (TM) format using the *TetGen* code (Si 2015) and the converted phantoms were implemented in Geant4 using the *G4Tet* class (Yeom *et al* 2014). Moreover, the ICRP-100 and ICRP-66 stylized models were implemented in the Geant4 code using the *G4Tube* and *G4Sphere* classes.

Note that the CSG-format airway models developed in the present study need to be converted to the PM format for incorporation into the PM phantoms. For this, however, a large number of polygonal facets, eventually tetrahedrons, would be necessary to represent the airways, requiring a huge memory consumption (>~50 GB), which is, at least at this point, impractical. Therefore, in the present study, the mesh phantoms were overlaid with the CSG lung airways in the Geant4 code by using *G4VUserParallelWorld* class, which is used for implementation of hierarchically-overlapped multiple geometries called 'parallel geometries' (Apostolakis *et al* 2008). Although available only in Geant4, this approach enables us to perform dose calculation for the detailed CSG lung airways with a minimal addition of memory usage.

Table 3. Length of the branches for each airway generation and their deviation from the reference value.

Generation	Reference branch length (cm)	Left lung (cm)		Right lung (cm)	
		Male (% diff.)	Female (% diff.)	Male (% diff.)	Female (% diff.)
2	3.00	2.74 (8.8)	3.09 (9.9)	2.92 (2.7)	3.00 (6.6)
3	3.32	3.62 (9.2)	3.39 (9.1)	3.65 (9.8)	3.40 (9.7)
4	7.20	7.42 (3.1)	6.67 (1.9)	7.09 (1.5)	7.13 (4.8)
5	12.96	13.38 (3.3)	12.37 (1.7)	12.98 (0.2)	12.94 (6.4)
6	21.12	21.26 (0.7)	21.21 (6.5)	22.44 (6.2)	20.18 (1.3)
7	38.40	38.74 (0.9)	37.36 (2.0)	40.33 (5.0)	37.48 (2.4)
8	67.84	66.80 (1.5)	64.19 (1.9)	66.57 (1.9)	67.93 (3.8)
9	111.80	111.59 (0.2)	111.10 (3.2)	109.92 (1.7)	104.42 (3.0)
10	185.34	185.51 (0.1)	180.64 (1.5)	190.74 (2.9)	178.94 (0.5)
11	308.12	303.41 (1.5)	289.58 (1.9)	314.97 (2.2)	288.78 (2.2)
12	512.00	512.71 (0.1)	487.58 (0.3)	520.68 (1.7)	491.57 (0.5)
13	847.46	834.54 (1.5)	793.37 (1.6)	825.46 (2.6)	794.28 (1.5)
14	1392.64	1373.73 (1.4)	1327.02 (0.6)	1398.72 (0.4)	1281.03 (2.9)
15	2260.99	2232.82 (1.2)	2094.01 (1.6)	2236.80 (1.1)	2135.43 (0.4)

Table 4. The target region of respiratory tract model of the mesh-type ICRP reference phantoms and ICRP-66 stylized models.

Target region	Depth of target cell (μm)	Male			Female		
		Mass (g)		Ratio (A/B)	Mass (g)		Ratio (A/B)
		Mesh (A)	ICRP-66 (B)		Mesh (A)	ICRP-66 (B)	
ET_1	40–50	2.81×10^{-2}	2.00×10^{-2}	1.41	1.09×10^{-2}	1.73×10^{-2}	0.63
ET_2	40–50	9.77×10^{-2}	4.50×10^{-1}	0.22	7.22×10^{-2}	3.89×10^{-1}	0.19
BB basal	35–50	3.83×10^{-1}	4.32×10^{-1}	0.89	3.03×10^{-1}	3.89×10^{-1}	0.78
BB secretory	10–40	7.53×10^{-1}	8.65×10^{-1}	0.87	6.00×10^{-1}	7.77×10^{-1}	0.77
bb secretory	4–12	1.69	1.95	0.87	1.49	1.74	0.86

Monoenergetic primary electrons were uniformly generated in the source regions of the TM phantoms using a sampling method based on the barycentric coordinate system of the tetrahedrons (Rocchini *et al* 2000). The electron sources of the CSG airway models were modeled by using the rejection method. The AI electron sources were also modeled using the rejection method but with a binary search tree (BST) algorithm to reduce computation time. For the stylized models, the corresponding electron sources were modeled using the *G4ParticleGun* class. The deposited energy to the target regions was calculated using the *G4PSEnergyDeposit* class. The deposited energy was then divided by the energy of the primary electrons to calculate the absorbed fraction (AF), which is then divided by the target mass to obtain the SAF value.

The primary electron energies ranging from 0.15 MeV to 4.0 MeV were considered in the SAF calculation for the alimentary tract organs. The energies less than 0.15 MeV were not considered due to the fact that these low-energy electrons do not reach the target regions for most exposure cases and therefore secondary photons from the electrons only contribute to the energy deposition to the target regions, which is almost negligible. For the respiratory tract organs, the primary electron energies ranging from 0.01 MeV to 4.0 MeV were preferentially

considered, but different lowest energies were considered for different exposure cases on which the negligible energy regions depend.

The number of primary electrons varied from 10^6 to 10^9 depending on the geometries and energies to keep the relative errors under 5%. The physics library of the *G4EmLivermorePhysics*, including EPDL97 (Cullen *et al* 1997), EEDL (Perkins *et al* 1991), and EADL (Perkins *et al* 1997), was used. A secondary range cut value of 1 μm was applied to both photons and electrons considering the micron scales of thin target layers. In the present study, a user limit of a maximum step length to electrons was not used, considering that in a previous study we found that the dose values were not changed within statistical uncertainty even though the user limit of the maximum step length to electrons was set as 0.4 μm, which is 20 times smaller than the thinnest target layer (=8 μm at bb regions). The simulations were performed on a single core of the AMD Opteron™6176 (@ 2.3 GHz and 256 GB memory).

3. Results and discussion

In the present study, the electron SAF values for the alimentary and respiratory tract systems were calculated with the mesh-type phantoms including the thin target and source regions, and the calculated values were compared with those of the ICRP-100 and ICRP-66 stylized models in order to investigate dose differences caused by the different topology and dimension of the alimentary and respiratory tract systems between the mesh phantoms and the stylized models. In addition, the SAF values were also compared to those published in ICRP *Publication* 133 (ICRP 2016).

3.1. Electron SAFs for alimentary tract organs

Figure 6 shows the calculated electron SAF values of the mesh phantoms to the oral mucosa, along with the values calculated with the ICRP-100 stylized phantom. For the food as source, the calculated SAF values for both the male and female mesh phantoms showed good agreement with those of the ICRP-100 stylized models: the maximum differences were 11.9% at 3.0 MeV and 18.3% at 4.0 MeV for the male and female, respectively.

For radionuclides retained on the surface of teeth, larger differences were observed: the maximum differences were 24.1% at 1.0 MeV and 56.7% at 0.8 MeV for the male and female, respectively. These relatively large differences are due mainly to the geometrical difference of the oral cavity between the mesh phantoms and the ICRP-100 stylized models. This discrepancy is, however, relatively unimportant in practice because radionuclides retained on the surface of teeth is ignored in most cases. The radionuclide retention is considered only when specific information on retention is available (ICRP 2006). Furthermore, the dose to the oral mucosa has been assigned a small tissue weighting factor (w_T), being classified as remainder tissue (ICRP 2007) and its contribution to the effective dose is therefore small.

Similarly, figure 7 shows the electron SAF values to the oesophagus for two source cases: fast and slow. The fast case is that radionuclides are uniformly distributed in the content. The slow case is that radionuclides are retained on the lumen surface of the oesophagus. It can be seen that the SAFs do not show significant differences between the mesh phantoms and the ICRP-100 stylized phantom. For the 'fast' case, and electron energies higher than 0.3 MeV, the SAF values for both male and female phantoms showed good agreement with those of the ICRP-100 stylized models: the maximum differences were only 5.9 and 7.4% at 0.5 MeV for the male and female, respectively. For the low energies ($\leqslant$0.3 MeV), the differences were slightly larger: the maximum differences were 21.9 and 31.0% at 0.15 MeV for the male and

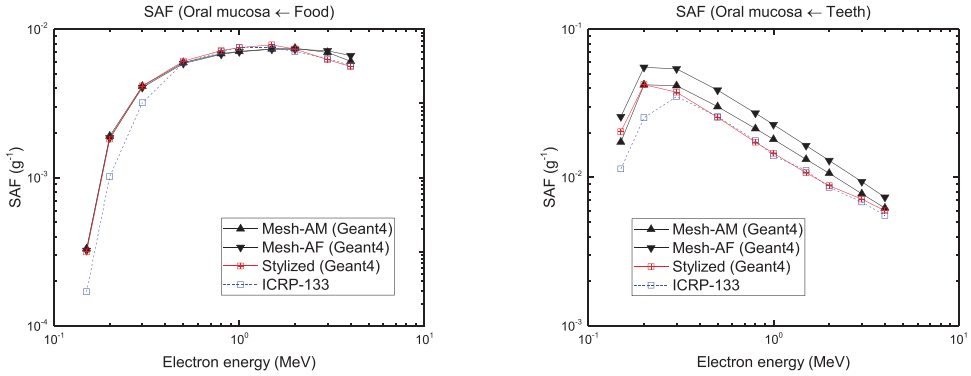

Figure 6. Specific absorbed fractions (SAFs) to the oral mucosa for electron exposures within mesh-type male phantom (filled black upward triangles), mesh-type female phantom (filled black downward triangles), ICRP-100 stylized model (unfilled red squares with cross), and ICRP-133 values (unfilled blue squares).

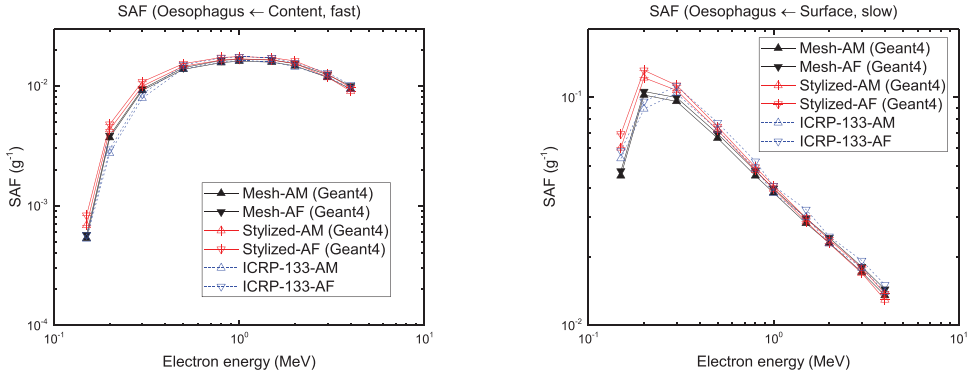

Figure 7. Specific absorbed fractions (SAFs) to the oesophagus for electron exposures within mesh-type male phantom (filled black upward triangles), mesh-type female phantom (filled black downward triangles), ICRP-100 stylized male model (unfilled red upward triangles with cross), ICRP-100 stylized female model (unfilled red downward triangles with cross), ICRP-133 male values (unfilled blue upward triangles), and ICRP-133 female values (unfilled blue downward triangles).

female, respectively. For the 'slow' case, the trend of the results was similar to that of the 'fast' case. For the energies greater than 0.3 MeV, the differences were all less than 7.9%, and for energies $\leqslant$0.3 MeV, the differences were higher than 10%, the maximum being 31.2% at 0.15 MeV for the female.

These slightly larger differences at low energies are due mainly to the difference in material composition between the mesh phantoms and the ICRP-100 stylized models. Note that the contents in the ICRP-100 phantoms are assumed to be water, while the mesh phantoms use the composition of the gastrointestinal contents given in the ICRP-89 reference data (ICRP 2002). For the low-energy electrons with a very short range, the dose to the target region is mainly contributed from the secondary photons, not from the short-range primary electrons, in which case, the material composition of the contents plays an important role.

Figure 8 shows the electron SAFs to the stomach for contents and mucosa as sources. It can be seen that, for the entire energy range, the SAF values of the mesh phantoms are smaller

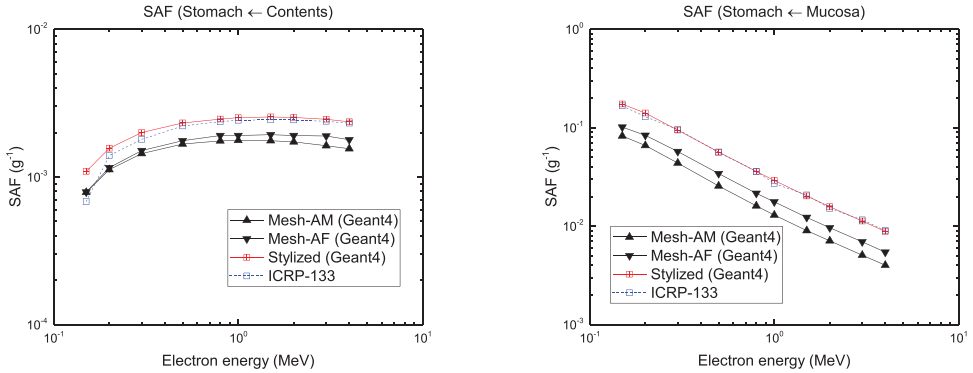

Figure 8. Specific absorbed fractions (SAFs) to the stomach for electron exposures within mesh-type male phantom (filled black upward triangles), mesh-type female phantom (filled black downward triangles), ICRP-100 stylized model (unfilled red squares with cross), and ICRP-133 values (unfilled blue squares).

than those of the ICRP-100 stylized phantom for both sources. The maximum differences were 34 and 55% for the contents and mucosal region, respectively. The smaller SAF values for the mesh phantoms are due mainly to the fact that their target masses are larger than those of the stylized phantom (see table 2). Note that for SAF calculation, the absorbed fraction (AF) is divided by the target mass and, therefore, the SAF value tends to be inversely proportional to the target mass. The difference in the target mass between the mesh phantoms and the stylized phantom is mainly caused by the difference in the lumenal dimension, more specifically the lumenal surface area determining the target mass. The lumens of the mesh phantoms, which are the result of the direct conversion from the voxel-type ICRP-110 reference phantoms, have a realistic shape and the lumenal volumes also match the ICRP-89 reference values (ICRP 2002). Note that the ICRP-89 reference values of the contents (=250 cm^3 and 230 cm^3 for male and female, respectively) were derived by estimating the average contents over a 24 h period (ICRP 2002), which we believe is reasonable for SAF calculation. For the stylized phantom, on the other hand, the lumen has a simple spherical shape and the lumenal volume was arbitrarily assumed to be 175 cm^3, i.e. without clear explanation or ground, which is not in accordance with the ICRP-89 reference values.

Figure 9 shows the SAFs to the small intestine for small intestine contents, mucosa, and villi as sources. In this case, the SAF values of the mesh phantoms were greater than those of the ICRP-100 stylized models for all of the source cases. For the retentions inside the mucosa and villi, the maximum differences were as large as ~1.8 and ~1.7 times, respectively; these differences are again due mainly to the difference of the target masses between the mesh phantoms and the stylized models due to the different lumen dimensions. As shown in table 2, the target masses of the mesh phantoms are smaller than those of the stylized models. For the contents as source, the differences in the SAF values were more significant than for the case of retention in mucosa and villi: the maximum difference was as large as ~2.9 times at 0.5 MeV, for the female. The SAF differences for the contents as source are caused by the differences in both target mass and content size between the mesh phantoms and the stylized models. In general, for larger contents, more of emitted electron energy is absorbed in the contents (i.e. self-absorption), and thus the AF value tends to be smaller. As shown in table 1, the content masses of the mesh phantoms match the ICRP-89 reference values of the small-intestine contents, whereas those of the stylized models do not, but are significantly larger than the reference values. Note that these SAF differences of the small intestine do not significantly

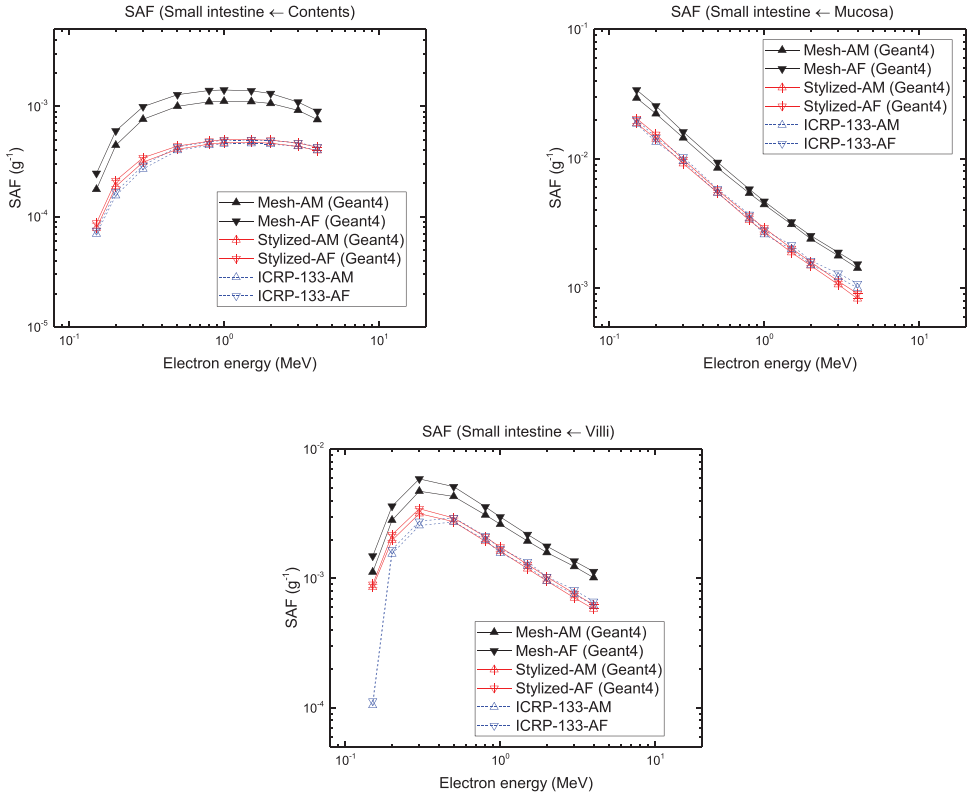

Figure 9. Specific absorbed fractions (SAFs) to the small intestine for electron exposures within mesh-type male phantom (filled black upward triangles), mesh-type female phantom (filled black downward triangles), ICRP-100 stylized male model (unfilled red upward triangles with cross), ICRP-100 stylized female model (unfilled red downward triangles with cross), ICRP-133 male values (unfilled blue upward triangles), and ICRP-133 female values (unfilled blue downward triangles).

affect effective dose calculation because the small intestine, classified as remainder in ICRP *Publication 103* (ICRP 2007), is not considered to be very sensitive to radiation.

Figure 10 shows the SAF results for the large intestine, which is divided into three parts: right colon, left colon, and rectosigmoid. Similar to the small-intestine case, the SAF values of the mesh phantoms were greater than those of the ICRP-100 stylized models, but the differences were more significant. For the retention in mucosal tissue, the maximum differences were as large as ~2.9, ~4.1, and ~2.4 times for the right colon, left colon and rectosigmoid, respectively. These differences are once again due mainly to the difference of the target masses between the mesh phantoms and stylized models (see table 2). For the contents as source, the differences were again more significant than those for the mucosa as source: the maximum differences were as large as ~6.2, ~9.2, and 3.4 times for the right colon, left colon, and rectosigmoid, respectively. These more significant differences are again caused by the differences in both the target mass and the content volume. Note that the content masses of the mesh phantoms are matched to the ICRP-89 reference values but that those of the stylized models are not, being significantly larger than the reference values (see table 1).

Figures 6–10 also show the new SAF values recently published in ICRP *Publication 133* (ICRP 2016). The ICRP-133 SAF values were calculated by using the ICRP-100 stylized

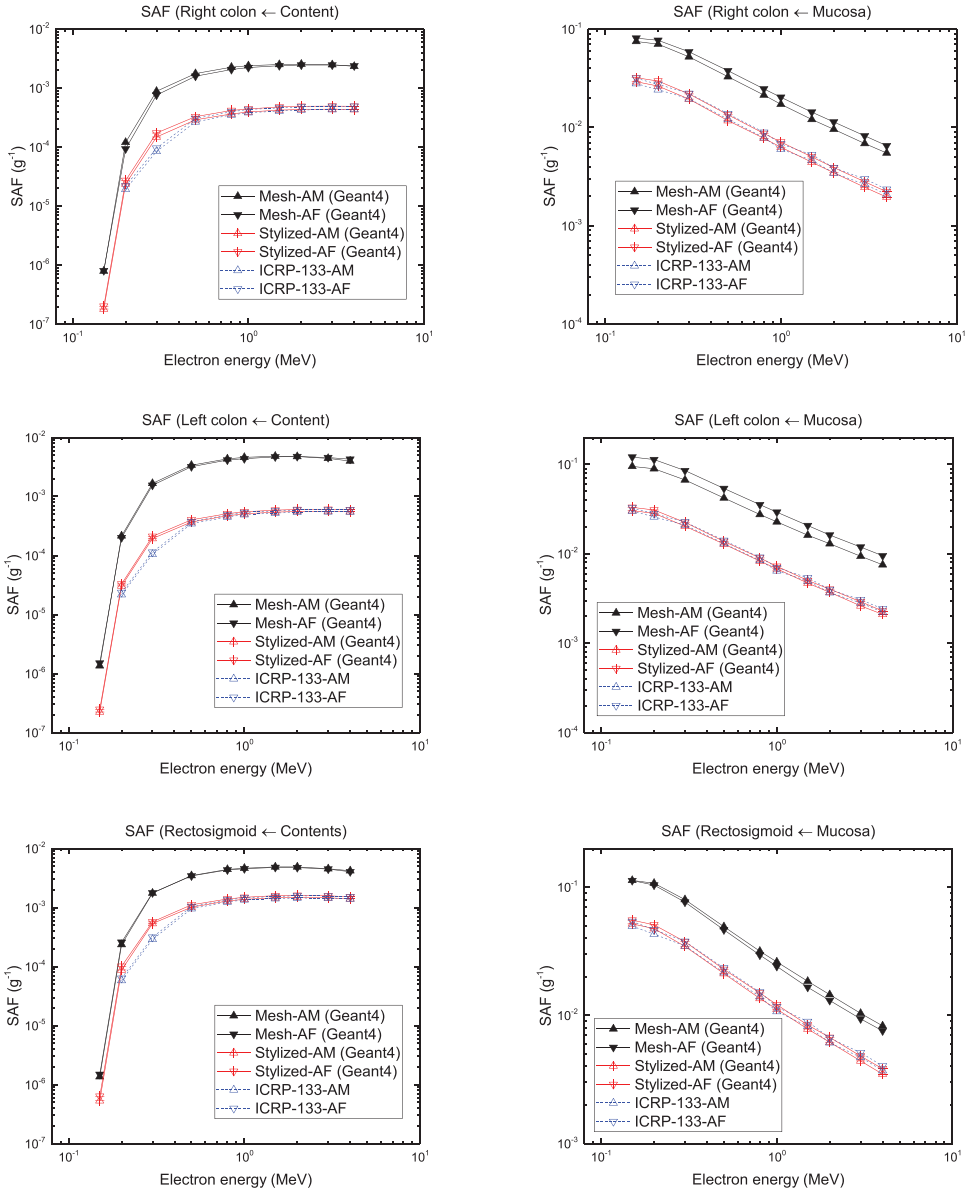

Figure 10. Specific absorbed fractions (SAFs) to the large intestine for electron exposures within mesh-type male phantom (filled black upward triangles), mesh-type female phantom (filled black downward triangles), ICRP-100 stylized male model (unfilled red upward triangles with cross), ICRP-100 stylized female model (unfilled red downward triangles with cross), ICRP-133 male values (unfilled blue upward triangles), and ICRP-133 female values (unfilled blue downward triangles).

models with one exception, which is the small intestine model. The ICRP-100 small intestine model is a single tubular structure, whereas the ICRP-133 model is a hexagonal array of tubular structures to allow for wall segment cross-fire. It can be seen that the ICRP-133 SAF values were generally in good agreement with those calculated by using the ICRP-100

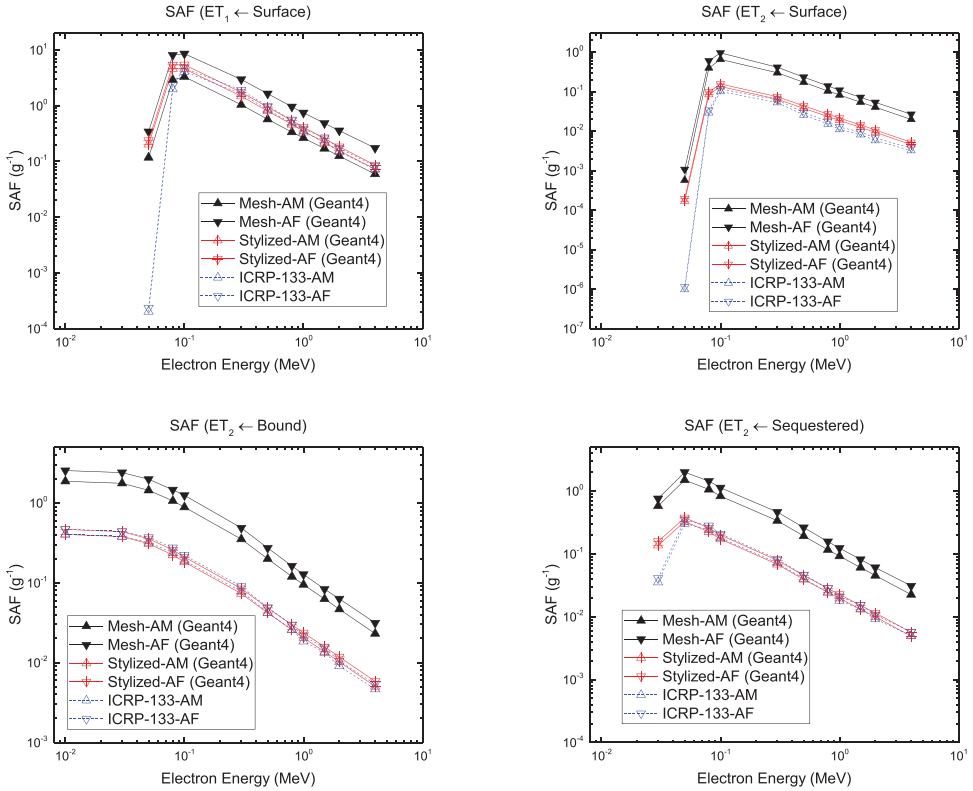

Figure 11. Specific absorbed fractions (SAFs) to the ET region for electron exposures within mesh-type male phantom (filled black upward triangles), mesh-type female phantom (filled black downward triangles), ICRP-66 stylized male model (unfilled red upward triangles with cross), ICRP-66 stylized female model (unfilled red downward triangles with cross), ICRP-133 male values (unfilled blue upward triangles), and ICRP-133 female values (unfilled blue downward triangles).

stylized models in the present study. Even though the ICRP-133 SAF values for the small intestine were calculated with the revised stylized models (ICRP 2016), the revision did not significantly affect SAF values in general. For some cases, however, relatively large discrepancies can be seen especially in low-energy electrons, which, we believe, are mainly due to the different electron physics models between MCNPX (ver. 2.6) used in ICRP *Publication 133* (ICRP 2016) and Geant4 used in the present study.

3.2. Electron SAFs for respiratory tract organs

Figure 11 shows the SAFs to the ET regions for the three source regions: surface (distributed on the inner surface of the airway), bound (material chemically bound in the airway wall), and sequestered (particles sequestered by macrophages in the lamina propria). It can be seen that for the ET_1 region, the SAFs of the mesh phantoms were different from those of the stylized models; the maximum differences were as large as about 1.7 and 2.1 times for the male and female, respectively. For the ET_2 region, the differences in SAFs were more significant than those for the ET_1 region; the maximum differences were as large as about 6.2, 5.9, and 5.8 times for three source cases (i.e. surface, bound, and sequestered), respectively. These

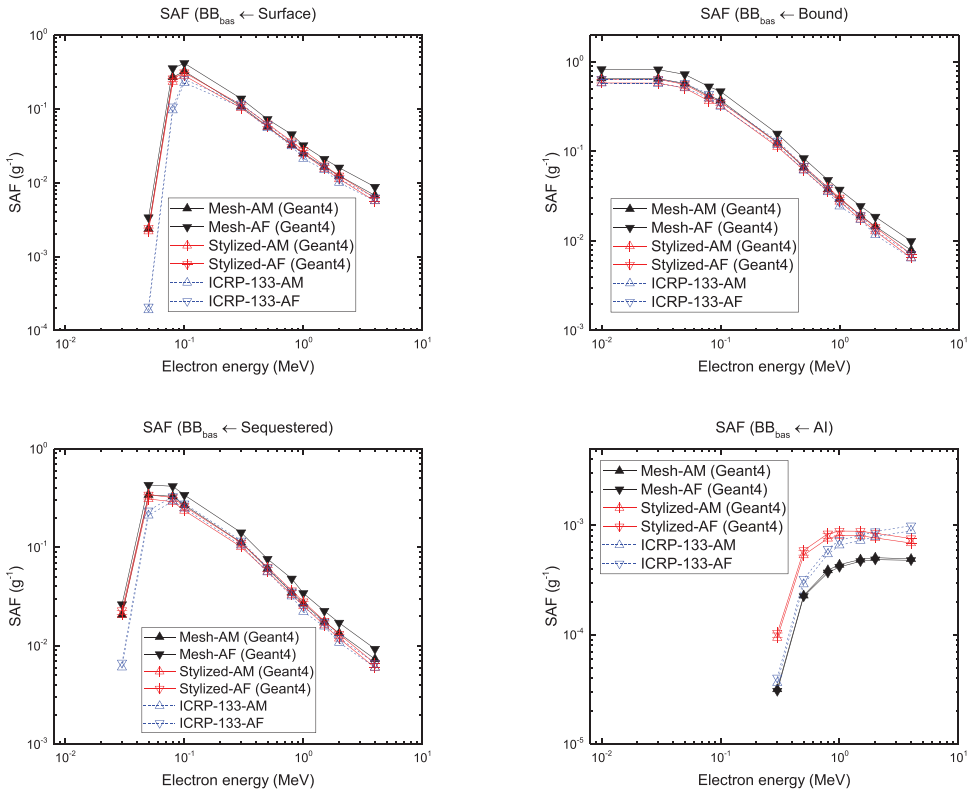

Figure 12. Specific absorbed fractions (SAFs) to the BB_{bas} target region for electron exposures within mesh-type male phantom (filled black upward triangles), mesh-type female phantom (filled black downward triangles), ICRP-66 stylized male model (unfilled red upward triangles with cross), ICRP-66 stylized female model (unfilled red downward triangles with cross), ICRP-133 male values (unfilled blue upward triangles), and ICRP-133 female values (unfilled blue downward triangles).

differences in SAF values for the ET regions are again due mainly to the differences of the target masses between the mesh phantoms and the stylized models (see table 4), which are due to the different shapes and dimensions (i.e. inner surface areas) between the ET models of the mesh phantoms and the stylized models. Considering that the ET models of the mesh phantoms maintain the ET shape of the ICRP-110 phantoms, we believe that the mesh phantoms provide more reliable dose values than the stylized models. Moreover, considering that the SAFs of the mesh phantoms for the ET_2 region were greater than those of the stylized models, the mesh phantoms always provide more conservative SAF values for the ET region. Note that the SAF differences in the ET_1 region, having a very small assigned fraction (=0.001) of the tissue weighting factor (ICRP 1994), do not significantly affect equivalent dose values for the ET region. Overall, we expect that the SAF differences for the ET region will not significantly affect effective dose calculations, considering that the ET is one of the remainder tissues (ICRP 2007) and that the clearance rate from ET_2 to alimentary tract is very fast (=100 d^{-1}) (ICRP 1994).

Figure 12 shows the SAF results for the BB_{bas} (basal cells) region as target and four source cases: surface, bound, sequestered, and AI. Note that the SAF values for the surface as a source are weighted averages of those for the original fast (gel) and slow (sol) regions as

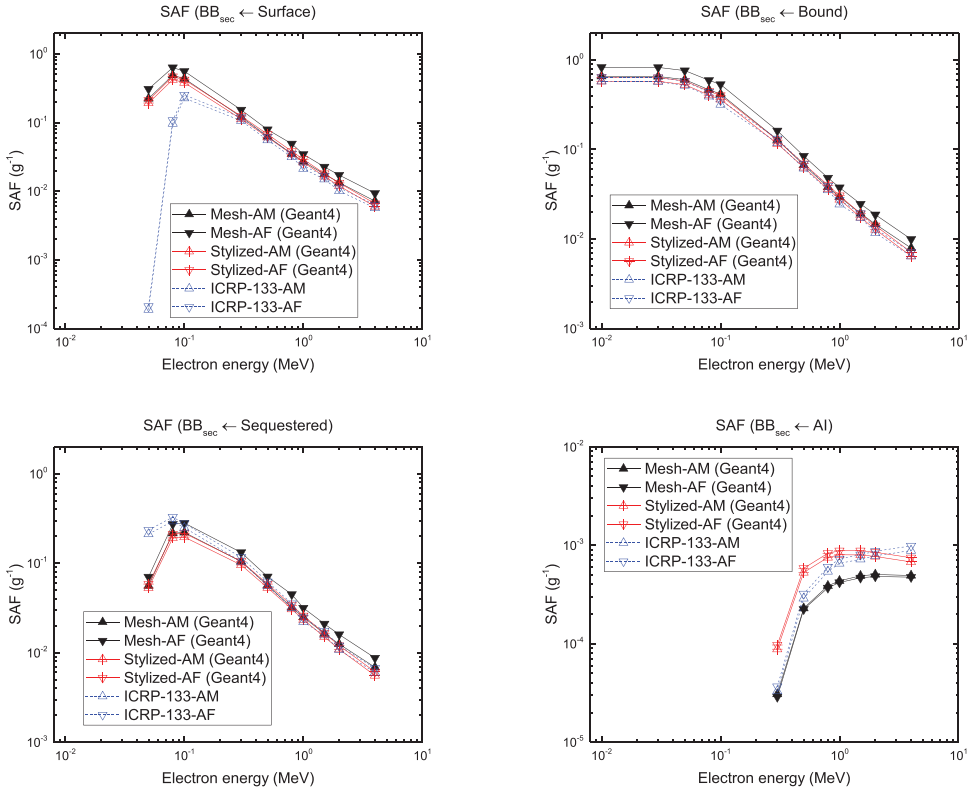

Figure 13. Specific absorbed fractions (SAFs) to the BB_{sec} target region for electron exposures within mesh-type male phantom (filled black upward triangles), mesh-type female phantom (filled black downward triangles), ICRP-66 stylized male model (unfilled red upward triangles with cross), ICRP-66 stylized female model (unfilled red downward triangles with cross), ICRP-133 male values (unfilled blue upward triangles), and ICRP-133 female values (unfilled blue downward triangles).

sources following the revised respiratory tract model (ICRP 2015, 2016). It can be seen that the differences in SAFs between the mesh phantoms and the stylized models were not significant for all source cases except for the AI: the differences for most cases were less than ~20 and ~30% for the male and female, respectively. These slight differences are again due mainly to the differences in the target masses. For the AI, on the other hand, there were significant differences; the maximum differences were as large as about 3.0 times and 3.4 times for the male and female, respectively. These significant differences are mainly due to the differences in the AI density between the mesh phantoms, i.e. the ICRP-110 phantoms (~0.4 g cm^{-3}) and the stylized models (0.2 g cm^{-3}). However, these SAF differences for the AI source would not significantly affect dose calculations, considering that the magnitude of the SAF values for the AI source is significantly smaller than that for the other source cases in general. Figure 13 also shows the SAF results for the BB_{sec} (secretory cells) region as target with observations similar to those for the BB_{bas} region.

Figure 14 shows the SAF results for the bb_{sec} (secretory cells) region as target. Except for the AI source region where significant SAF differences were found due to the different AI densities, it can be seen that an overall trend is similar for all source regions. For the energies (<0.5 MeV), the SAF values of the mesh phantoms show good agreement with those of the

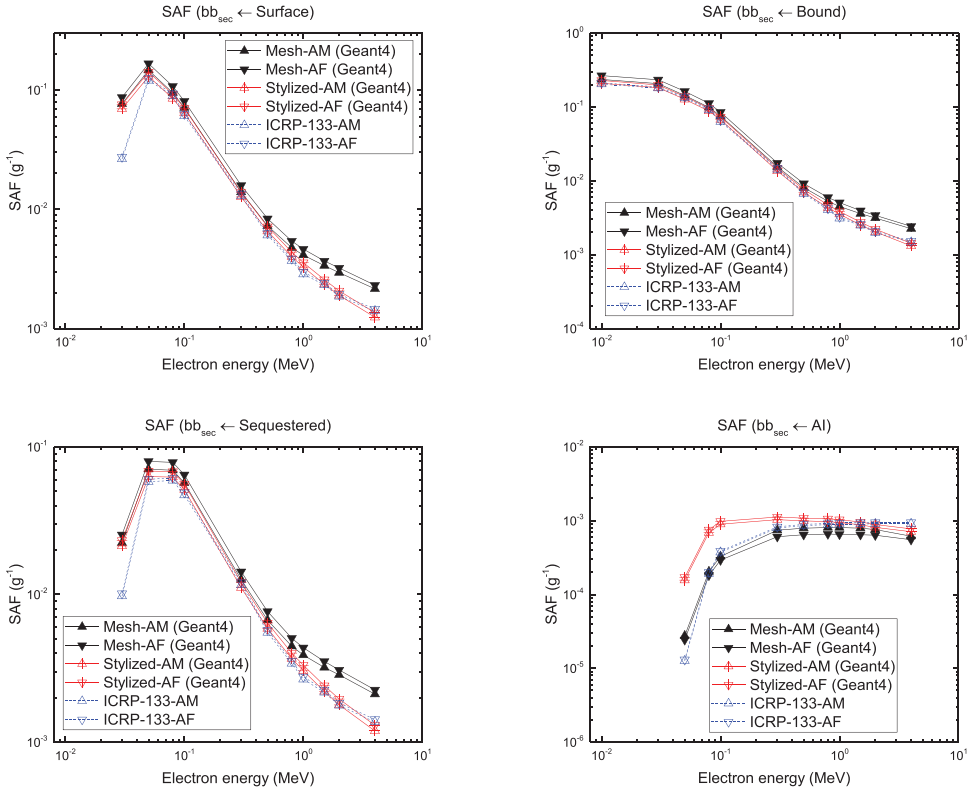

Figure 14. Specific absorbed fractions (SAFs) to the bb_{sec} target region as a target for electron exposures within mesh-type male phantom (filled black upward triangles), mesh-type female phantom (filled black downward triangles), ICRP-66 stylized male model (unfilled red upward triangles with cross), ICRP-66 stylized female model (unfilled red downward triangles with cross), ICRP-133 male values (unfilled blue upward triangles), and ICRP-133 female values (unfilled blue downward triangles).

stylized models; that is, the maximum differences were only 14% and 18% for the male and female, respectively. For the higher energies, on the other hand, significant differences can be found; the maximum differences were 77% and 74% for the male and female, respectively. These significant differences are due mainly to the different amount of dose contribution from cross irradiations of remote airways between the mesh phantoms and the stylized models. We believe that the mesh phantoms, with the realistic airways, provide more reliable dose values for the cross irradiations than the single-cylindrical-shape stylized models which cannot explicitly represent the cross-irradiation contributions. Although, for the stylized models, the surrogate calculated values of AF(bb ← AI) were already added to consider the cross-irradiation contribution in the calculation following the approach of the ICRP *Publication 66* (ICRP 1994), it is shown that this approach is not sufficient for the high energies, considering that the stylized-model-calculated SAF values for the surface, sequestered, and bound as sources were significantly smaller than the mesh-phantom-calculated SAF values.

Figures 11–14 also show the ICRP-133 SAF values calculated by using the ICRP-66 stylized models. It can be also seen that the ICRP-133 SAF values were generally in good agreement with those calculated by using the ICRP-66 stylized models in the present study. For some cases, relatively large discrepancies can be also seen especially in the low-energy

electrons, again due mainly to the different electron physics models between EGSnrc (ver. V4-2-3-0) used in ICRP *Publication 133* (ICRP 2016) and Geant4 used in the present study, with the only exception of the BB_{sec}. In the present study, we found that the ICRP-133 SAF values for the BB_{sec} were duplicated with those for the BB_{bas} for all source cases.

4. Conclusion

The ICRP has recently formed a Task Group under Committee 2 to convert the voxel-type ICRP reference phantoms to a high-quality mesh format in order to address the limitations of the voxel-type ICRP reference phantoms due to the limited voxel resolutions. As a part of the conversion project, in the present study, the thin target and source regions of the alimentary and respiratory tract organs were defined in the mesh-type ICRP reference phantoms currently under development. In addition, realistic airway models were produced to represent the BB and bb regions in the mesh phantoms. In order to investigate the dosimetric impact of this work, the electron SAF values for the alimentary and respiratory tract organs were calculated within the developed mesh phantoms and compared with those of the ICRP-100 and ICRP-66 stylized models. The results show that there is generally good agreement in SAF values for the oral cavity, oesophagus, and BB whereas for the stomach, small intestine, large intestine, ET, and bb, there are large differences mainly due to the different topology and dimensions of the mesh-type phantoms and stylized models. Considering that the mesh phantoms preserve the topology and dimensions of the alimentary and respiratory tract organs of the current ICRP reference phantoms, faithfully following the ICRP-89 reference data and also provide more realistic anatomy than the stylized models, it is believed that the new mesh phantoms provide more reliable SAF values than the stylized models.

Acknowledgments

This project was supported by the Nuclear Safety and Security Commission (NSSC) through the Korea Foundation of Nuclear Safety (KOFONS) and also by the Ministry of Science, ICT and Future Planning through the National Research Foundation of Korea (Project No.: 1403012, 2016R1D1A1A09916337). This work was also supported by ETRI R&D Program (Development of particle beam range verification technology based on prompt gamma-ray measurements, 15ZC1810) funded by the Government of Korea.

References

Agostinelli S *et al* 2003 GEANT4—a simulation toolkit *Nucl. Instrum. Methods* A **506** 250–303

Apostolakis J *et al* 2008 Parallel geometries in Geant4: foundation and recent enhancements *IEEE Nuclear Science Symp. Conf. Record (NSS '08)* pp 883–6

Behrens R, Dietze G and Zankl M 2009 Dose conversion coefficients for electron exposure of the human eye lens *Phys. Med. Biol.* **54** 4069–87

Cullen D, Hubbell J H and Kissel L 1997 EPDL97: the evaluated photon data library, '97 version *Lawrence Livermore National Laboratory* **6** UCRL-50400

ICRP 1994 Human respiratory tract model for radiological protection. ICRP publication 66 *Ann. ICRP* **24** 1–482

ICRP 2002 Basic anatomical and physiological data for use in radiological protection: reference values. ICRP publication 89 *Ann. ICRP* **32** 5–265

ICRP 2006 Human alimentary tract model for radiological protection. ICRP publication 100 *Ann. ICRP* **36** 25–327

ICRP 2007 The 2007 recommendations of the International Commission on Radiological Protection. ICRP publication 103 *Ann. ICRP* **37** 1–332
ICRP 2009 Adult reference computational phantoms. ICRP publication 110 *Ann. ICRP* **39** 1–164
ICRP 2010 Conversion coefficients for radiological protection quantities for external radiation exposures. ICRP publication 116 *Ann. ICRP* **40** 2–54
ICRP 2015 Occupational intakes of radionuclides: part 1. ICRP publication 130 *Ann. ICRP* **44** 5–188
ICRP 2016 The ICRP computational framework for internal dose assessment for reference adults: specific absorbed fractions. ICRP publication 133 *Ann. ICRP* **45** 1–74
Kim C H *et al* 2016 The reference phantoms: voxel versus polygon *Ann. ICRP* **45** 188–201
Kim C H, Jeong J H, Bolch W E, Cho K W and Hwang S B 2011 A polygon-surface reference Korean male phantom (PSRK-Man) and its direct implementation in Geant4 Monte Carlo simulation *Phys. Med. Biol.* **56** 3137–61
Lazaro S 2011 *Modelling of Realistic Blood Vessel Geometry* (Hannover: Gottfried Wilhelm Leibniz Universität)
Lee C, Lodwick D, Hasenauer D, Williams J L, Lee C and Bolch W E 2007 Hybrid computational phantoms of the male and female newborn patient: NURBS-based whole-body models *Phys. Med. Biol.* **52** 3309–33
Nguyen T T *et al* 2015 Incorporation of detailed eye model into polygon-mesh versions of ICRP-110 reference phantoms *Phys. Med. Biol.* **60** 8695–707
Perkins S T, Cullen D E and Seltzer S M 1991 Tables and graphs of electron-interaction cross-sections from 10 eV to 100 GeV derived from the LLNL evaluated electron data library (EEDL), $Z = 1$–100 *Lawrence Livermore National Laboratory* **31** UCRL-50400
Perkins S T, Cullen D E, Chen M H, Hubbell J H, Rathkopf J and Scofield J 1997 Tables and graphs of atomic subshell and relaxation data derived from the LLNL evaluated atomic data library (EADL), $Z = 1$–100 *LLNL Report No* UCRL-50400-v-30 Lawrence Livermore National Laboratory, Livermore, CA
Rocchini C and Cignoni P 2000 Generating random points in a tetrahedron *J. Graph. Tools* **5** 9–12
Si H 2015 TetGen, a delaunay-Based quality tetrahedral mesh generator *ACM Trans. Math. Soft.* **41** 36
Tawhai M H, Pullan A J and Hunter P J 2000 Generation of an anatomically based three-dimensional model of the conducting airways *Ann. Biomed. Eng.* **28** 793–802
Yeom Y S, Han M C, Kim C H and Jeong J H 2013 Conversion of ICRP male reference phantom to polygon-surface phantom *Phys. Med. Biol.* **58** 6985–7007
Yeom Y S *et al* 2016a Development of skeletal system for mesh-type ICRP reference adult phantoms *Phys. Med. Biol.* **61** 7054
Yeom Y S *et al* 2016b New small-intestine modeling method for surface-based computational human phantoms *J. Radiat. Prot.* **36** 230
Yeom Y S, Jeong J H, Han M C and Kim C H 2014 Tetrahedral-mesh-based computational human phantom for fast Monte Carlo dose calculations *Phys. Med. Biol.* **59** 3173–85